Food Chemistry: X 15 (2022) 100404

Contents lists available at ScienceDirect

Food Chemistry: X

journal homepage: www.sciencedirect.com/journal/food-chemistry-x

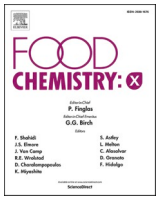

Biochar-supported Cu nanocluster as an electrochemical ultrasensitive interface for ractopamine sensing

Yanan Lei [a,b,1], Yuhuan Zhang [a,b,1,*], Li Yuan [a,b], Jianke Li [a,b,*]

[a] College of Food Engineering and Nutritional Science, Shaanxi Normal University, Xi'an 710119, China
[b] University Key Laboratory of Food Processing Byproducts for Advanced Development and High Value Utilization, Xi'an 710119, China

ARTICLE INFO

Keywords:
Ractopamine
Electrochemical sensors
Carbon nanofibers
Cu nanocluster
Ultrasensitive detection

ABSTRACT

Electrochemical sensors actually involve an electrocatalytic process involving an efficient and selective energy conversion that is related to the morphology and size of the interface of the modified materials. Ultrasmall nanoclusters or single atoms generate a greater catalytic ability than normal nanomaterials. In this study biochar-supported Cu nanoclusters (CuNCs@CNFs) were fabricated via a carbon confinement synthesis method toward ultrasensitive electrochemical sensing of ractopamine (RAC). RAC is a β-adrenergic receptor agonist that is illegally used as a feed additive to significantly improve muscle accretion, resulting in RAC accumulation in meat-based food products. The unique structure of CuNCs@CNFs and the interconnectivity between the CuNCs and the CNFs enable the nanocomposite to significantly enhance conductivity and electrocatalytic activity. Using the CuNCs@CNFs-based sensor, RAC was determined with a high sensitivity of 1641 μA μM^{-1} cm^{-2}. The feasibility of detecting RAC in spiked meat samples was also carried out with satisfactory recoveries ranging from 91.39 % to 94.58 %.

1. Introduction

Ractopamine (RAC) is classified as a β-adrenergic receptor agonist. RAC was originally developed for the treatment of pulmonary disease and asthma. However, today it is illegally used in animal feed to enhance muscle content and decrease adipose tissue deposition in order to increase muscle growth rate (Armstrong et al., 2004). Mounting evidence has demonstrated that excessive intake of RAC causes adverse health effects such as acute poisoning, nervousness, and cancers (He et al., 2011; Rajkumar et al., 2013; Liu et al., 2012). To date, RAC has been banned or restricted in 160 countries, including China, members of the European Union (EU) and Russia. While in some countries RAC is widely used, it is estimated that 60 %-80 % of pigs raised are fed the RAC (Aroeira et al., 2021). Due to the high risk of RAC, the Codex Alimentarius Commission (CAC) adopted the first-ever maximum residue levels (MRL) for RAC hydrochloride as 10 μg kg^{-1} for beef and pork in 2012. The U.S. Environmental Protection Agency (EPA) has adopted a 2.5 mg L^{-1} maximum RAC contaminant level for meat, and the World Health Organization (WHO) standard for the maximum permissible levels of RAC in meats is 5 mg kg^{-1} (Bai et al., 2014). China and the EU do not tolerate residues of the RAC in meat. Nevertheless, the illegal addition of RAC has been consistently reported (Zhang et al., 2022; Liu et al., 2022b). For example, the Rapid Alert System for Food and Feed (RASFF) of the EU reported RAC residue in beef livers in 2012. Chinese custom detected RAC residue in imported beef and pork in 2017 and 2019. Therefore, the ultrasensitive monitoring of RAC in food is of significant importance for food safety and human health.

To date, various methods for RAC detection have been established (Simon et al., 2018; Han et al., 2021; Muthumariyappan et al., 2019), among which electrochemical methods are advantageous for their ease of operation, rapid response, high sensitivity, and suitability for rapid sensitive detection and spatial–temporal analysis (Poo-arporn et al., 2019; Shen et al., 2022). Untill now, different electrochemical methods have been reported for the monitoring of RAC in food samples (Liu et al., 2012; Muthumariyappan et al., 2019).

However, the sensitive electrochemical detection of RAC in food is still challenging, due to their high overpotential as well as poor response signals of RAC on ordinary electrode surfaces (Wu et al., 2012). Modifying nanomaterials with high electrocatalytic activity on the surface of electrodes is regarded as the most effective way to enhance the sensing performance of electrochemical sensors. Nanomaterials such as metal or metal oxide nanoparticles (Bai et al., 2022; Wang et al., 2020),

* Corresponding authors at: College of Food Engineering and Nutritional Science, Shaanxi Normal University, Xi'an 710119, China.
E-mail addresses: yh5zhang@snnu.edu.cn (Y. Zhang), jiankel@snnu.edu.cn (J. Li).
[1] These authors are contributed equally.

https://doi.org/10.1016/j.fochx.2022.100404
Received 2 May 2022; Received in revised form 8 July 2022; Accepted 24 July 2022
Available online 1 August 2022

metal–organic framework (MOF) (Yue et al., 2022), carbon nanomaterials (Vatandost et al., 2020), etc. with large surface areas, numerous electrochemical active sites, and fast electron-transfer kinetics are the most promising candidates. Among them, transition metal nanomaterials such as CuO (Sudha et al., 2018), $FePO_4$ (Wang et al., 2018), $Mn_3(PO_4)_2$ (Zhang et al., 2015), ZrO_2 (Rajkumar et al., 2013) and Co_3O_4 (Xia et al., 2014) have been used for the sensitive electrochemical detection of RAC due to their abundant reserves, low manufacturing cost, and high catalytic ability. Moreover, electrochemical sensors utilize an electrocatalytic process needed for the efficient and selective energy conversion which is primarily related to the morphologies and size of the interface of the modified materials (Zhang et al., 2019). Ultrasmall nanoclusters or single atoms (SAs) generally generate greater catalytic ability than normal nanomaterials because of high atom utilization and prominent size effects (Singh et al., 2021; Wang et al., 2017). Yet the fabrication of SAs faces significant challenges since the SAs cluster easily under real working conditions (Singh et al., 2021). Studies have proven that porous carbon nanofibers (CNFs) can produce space confinement effects during the *in situ* carbon reduction of metal ions, prevent the gathering of nanoparticles and further increase of nanoparticles size, forming tiny nanoclusters, as well as endowing the electrode materials with numerous defects, large surface areas, high electrical conductivity, and many mass/ion transfer channels (Liu et al., 2019; Kang et al., 2022; Xiao et al., 2022). CNFs are, therefore, ideal supporters for the synthesis of nanoclusters needed in order to develop electrochemical sensor platforms with high performance.

Herein, we report the fabrication of an ultrasensitive and selective detection method of RAC in food using a novel biochar-supported Cu nanocluster (CuNCs@CNFs) constructed via a carbon confinement synthesis method. Porous CNFs in this work provide a space confinement effect during the *in situ* carbothermic reduction of Cu^{2+}, resulting in tiny CuNCs, which act as supporters and reductants of CuNCs. In the sensing of RAC, the synergistic effects of CNFs with superior conductivity and mesopore structure, the CuNCs with high electrocatalytic activity, and the interconnectivity between CuNCs and CNFs allowed for the high sensing performance of the CuNCs@CNFs. A linear response from 2 to 850 nM with a lower limit of detection (LOD) of 0.05 nM, and an ultrahigh sensitivity of 1641 $\mu A\ \mu M^{-1}\ cm^{-2}$ were experimentally observed using CuNCs@CNFs-based sensors. The feasibility of detecting RAC in different kinds of meat was successfully carried out with satisfactory recoveries ranging from 91.39 % to 94.58 %, which is comparable to that obtained using HPLC methods.

Material and methods

2.1. Chemicals and reagents

Copric chloride dihydrate ($CuCl_2{\cdot}2H_2O$, 99.99 %), dopamine (DA, 98 %), Glucose (Glu, 99.5 %), uric acid (UA, 99 %), clenbuterol (Cle, 1.0 mg/mL), fenoterol (Fen, 99 %), salbutamol (Sal, 95 %),

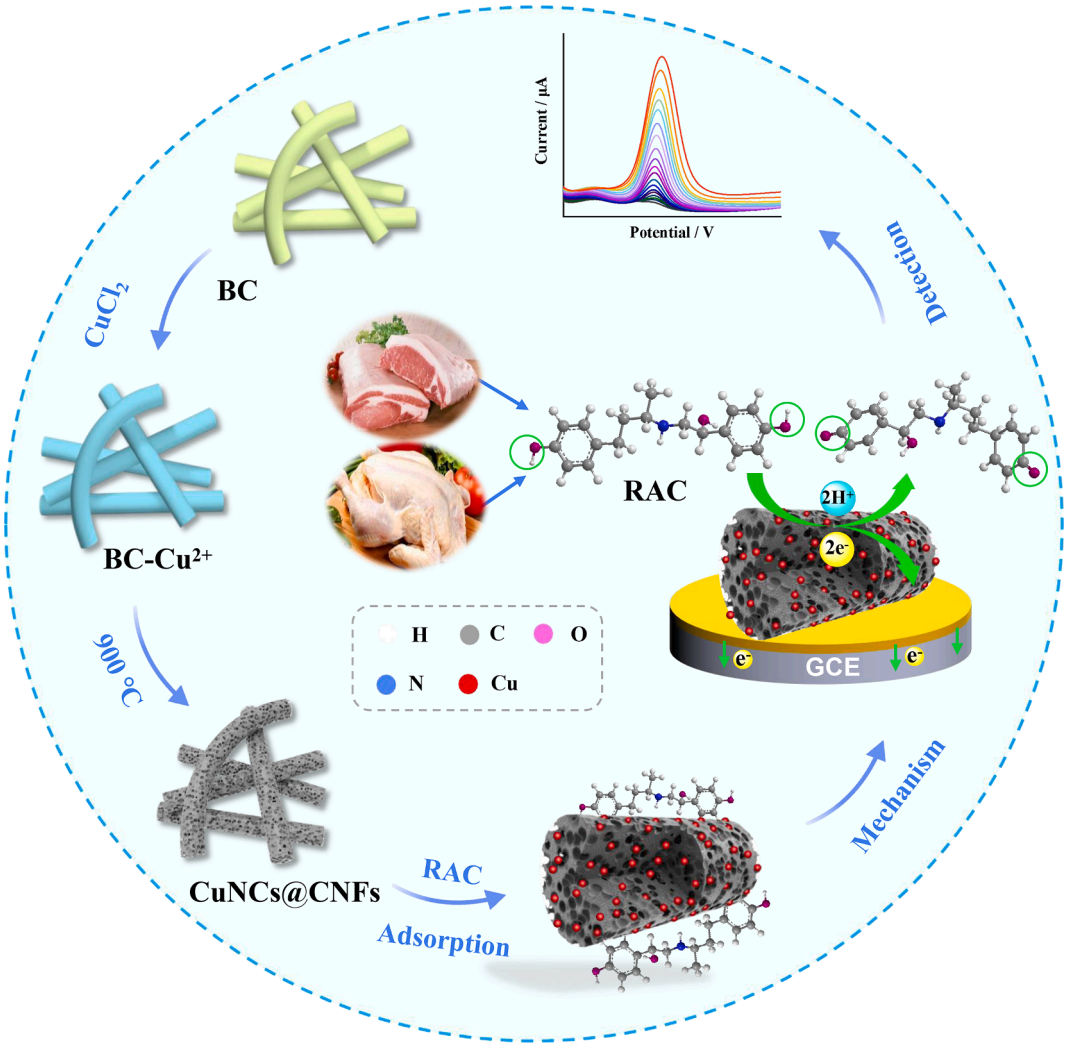

Scheme 1. The synthesis process of CuNCs@CNFs nanocomposite and electrochemical detection of RAC based on CuNCs@CNFs/GCE.

phenylethanolamine A (Phe, 98 %) and ascorbic acid (AA, 99 %) were purchased from Sigma-Aldrich, ractopamine (RAC) was purchased from Dr. Ehrenstorfer GmbH and used as received without any additional purification. All other reagents are of analytical grade and were purchased from Tianjin Tianli Chemical Reagent Co., ltd. (Tianjin, China). All solutions were prepared using ultrapure water (18.2 MΩ cm) and stored at 4 °C, deaerating with high-purity nitrogen before experiments. Bacterial cellulose (BC) was obtained by inoculating tofu yellow slurry water with *Acetobacter xylinum* followed by 5 day's culture (Tabuchi, et al., 1998).

2.2. Synthesis of CuNCs@CNFs

The synthesis process of CuNCs@CNFs is shown in Scheme 1. Firstly, BC was decolored with 0.1 M NaOH and washed with ultrapure water to neutral. Then, BC was soaked in 0.001 M $CuCl_2{\cdot}2H_2O$ for 12 h to acquire BC-Cu^{2+} by electrostatic adsorption of hydroxyl or carboxylic acid groups on BC to Cu^{2+}. After stirring continuously for 12 h, the BC-Cu^{2+} was washed 5 times with ultrapure water to remove excess Cu^{2+}. Then the BC-Cu^{2+} was dried in a vacuum freeze-drying equipment for 3 h. Finally, CuNCs@CNFs were obtained by carbonizing BC-Cu^{2+} at 900 ℃ for 1 h in nitrogen flow. The temperatures were started from room temperature to rise at 2℃ min^{-1} to 180℃, then at 1℃ min^{-1} to 500℃ and at 2℃ min^{-1} to 900℃, followed by cooling naturally to room temperature in nitrogen flow.

2.3. Apparatus

All electrochemical experiments were tested on a CHI660D electrochemical workstation (Chenhua, Shanghai, China). During all the tests, a platinum wire electrode was used as the counter electrode, an Ag/AgCl electrode was used as the reference electrode and a glassy carbon electrode (GCE, Ø = 3 mm) was used as the working electrode. Morphology of the as-prepared nanocomposites was investigated with field emission scanning electron microscope (FESEM, SU-8020, Hitachi, Japan) and transmission electron microscope (TEM, JEM-2800, Jeol, Japan). The crystallographic structure was carried out by X-ray diffraction (XRD, Smart Lab, Rigaku) with Cu Kα radiation in the 2θ range of 10°-90°. X-ray photoelectron spectroscopy (XPS) was performed by ESCALAB 250xi (Thermo Fisher Scientific, America). Energy-dispersive spectroscopy (EDS) was performed by X-Max 80/EX-270 (HORIBA, Japan).

2.4. Preparation of nanomaterials modified electrodes

The synthesized nanomaterials, CuNCs@CNFs and CNFs, were respectively dispersed in ethanol and ultrapure water (v/v = 1:1) to form a 3.0 mg/mL suspension. Subsequently, 5 μL of the above dispersed solution were respectively modified on the GCE surface and dried in air under room temperature. Before measurement, the used buffer solution, 0.01 M phosphate buffer saline (PBS, pH = 7.4), was purged with nitrogen for 10 min to remove dissolved oxygen, and the CuNCs@CNFs/GCE or CNFs/GCE were scanned in blank PBS buffer solution between 0.1 and 0.9 V at 50 mV/s until the cyclic voltammogram (CV) sweeps being steady to activate the electrodes.

2.5. Sample preparation

Meat purchased from market were used as detection samples. The preparation processes were carried out according to previous work (Wu et al., 2012; Keerthi et al., 2022). 2 g of meat sample was first crushed. 4 mL 0.1 M $HClO_4$ was then added to the crushed sample followed by ultrasonication for 30 min. The samples were kept in water at 80 ℃ for 30 min. Next, the supernatant of the above mixture was collected by centrifuging at 6000 rpm (4724 rcf) for 10 min. The obtained supernatants were extracted using 5 mL of ethylacetate after adjusting their pH to 10 with 0.01 M NaOH, then RAC was back-extracted into HCl solution. The extraction and extraction were repeated several times. Finally, the RAC solutions were diluted to 10 mL with PBS (0.01 M, pH 7.4).

3. Results and discussion

3.1. Characterization of CuNCs@CNFs

The morphology and microstructure of BC and the CuNCs@CNFs were visualized using FESEM (Fig. 1a, b). It revealed that the fiber network structure of BC (Fig. 1a) remained unchanged after the pyrolysis process except the surface became rougher (Fig. 1b). In Fig. 1c, numerous light spots that were dispersed in the TEM image of CuNCs@CNFs and labeled by red circles. These dispersed light spots are considered to be CuNCs with diameters of 1.25–2.75 nm (Fig. 1e). EDS imaging (Fig. 1d) revealed the co-existence of C, Cu, and N within the CuNCs@CNFs nanocomposite materials. The existence of C and Cu agrees with the elemental compositions of the CuNCs@CNFs, while the N element may have derived from the pristine BC that were cultured within the *N*-rich tofu yellow slurry water. The elemental composition of the CuNCs@CNFs is then investigated and characterized using XPS. The images reveal a wide survey spectra of the CuNCs@CNFs (Fig. 1f), showing that C and Cu co-exist on the surface of the CuNCs@CNFs. In the high-resolution Cu 2p spectrum, two main peaks with binding energies at 952.3 and 932.4 eV correspond to Cu $2p_{1/2}$ and Cu $2p_{3/2}$, respectively (Fig. 1h). The above characteristics confirmed the successful carbon confinement synthesis of CuNCs on the surface of the CNFs (Mahmoud and Haitham, 2022).

Furthermore, the crystal structure of the CuNCs@CNFs was investigated using the XRD spectrum (Fig. 1i). All diffraction peaks corresponding to the (1 1 1), (2 0 0), (2 2 0), and (3 1 1) planes of Cu (JCPDS no. 70–7038) (Liu et al., 2022a), except the broad diffraction peak of carbon at approximately 25°. The intense and sharp peaks of Cu suggested that the sample is of high purity and excellent crystallinity and agrees with the high-resolution TEM images (HRTEM) (inset of Fig. 1c). The pore size distribution of the CuNCs@CNFs was also tested using the nitrogen adsorption–desorption isotherms (Fig. S1). As shown in Fig. 1g, a certain number of mesoporous (2–50 nm) were present in CuNCs@CNFs, enabling the CuNCs@CNFs with an enlarged surface area and numerous channels for mass transport. The pyrolysis process endowed the carbon supports with porous structure, and also yields a thermal reduction environment for the synthesis of the CuNCs. More importantly, the mesopores within the CNFs effectively prevents the increase in size of the CuNCs due to providing a space-limiting environment.

3.2. Electrochemical properties of the CuNCs@CNFs.

The electrocatalytic performance of different materials used for RAC sensing was studied via CV curves measured in 0.01 M PBS (pH 7.4). Fig. S2 shows the CV signals of the CuNCs@CNFs/GCE sensor with and without 200 nM RAC. No visible signal peak appeared in the blank PBS; however, a very strong oxidation peak was observed at 0.56 V in the presence of RAC, indicating a relatively high electrocatalytic activity of the CuNCs@CNFs/GCE sensor for RAC oxidation. For comparison, CVs of different electrodes were measured in 0.01 M PBS containing 400 nM RAC (Fig. 2a). CuNCs@CNFs exhibited the highest peak current and lowest peak potential than other materials, while bare GCE generated the lowest current signal and highest peak potential. For an electro-oxidation reaction, a higher peak current symbols a larger surface reaction area. A more negative half-wave potential means a higher electrocatalytic activity (Zhang et al., 2021). Therefore, the CuNCs@CNFs were considered to have the highest electrooxidation catalytic ability and largest active surface area with respect to other nanomaterials. This can be attributed to the strong catalytic activity of Cu as well as the unique structure of the extra-small CuNCs located on the surface of the porous CNFs; thus, exposing significantly more Cu

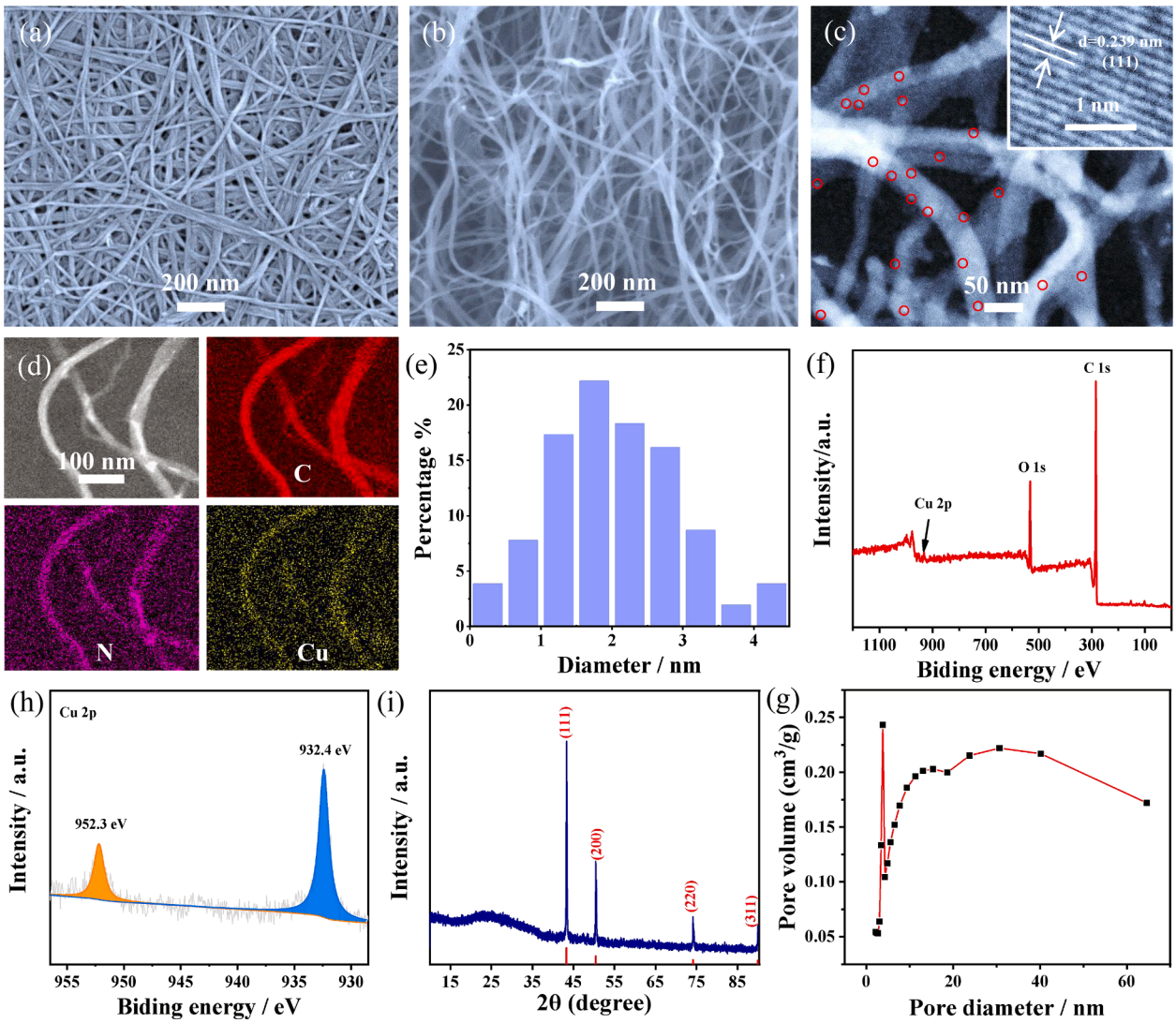

Fig. 1. FESEM images of (a) BC, (b) CuNCs@CNFs. (c) TEM image with inset of HRTEM of CuNCs@CNFs. (d) EDS mapping images of CuNCs@CNFs. (e) Particle size distribution chart of CuNCs. (f) XPS surveys spectrum and (h) high-resolution Cu 2p XPS spectra of CuNCs@CNFs. (i) XRD patterns of CuNCs@CNFs. (g) Pore size distribution curve of CuNCs@CNFs.

active sites.

In order to further verify the above results, a double layered capacitance (C_{dl}) that is proportional to the active surface area of the nanomaterial's modified electrodes was determined (Zhang et al., 2019). CVs of the CuNCs@CNFs/GCE, CNFs/GCE, and bare GCE were tested at various scan rates (10, 20, 30, 50, 60, 80, and 90 mV s^{-1}) in a potential window of 0.15–0.25 V where no apparent Faradaic processes occur (Fig. S3). Plots of the double layer currents at 0.2 V as a function of the scan rates of the three electrodes were illustrated in Fig. 2b, in which the slopes corresponding to their C_{dl} are 74.08, 14.73, and 5.51 μF for the CuNCs@CNFs, CNFs, and bare GCE, respectively. This again verified that the CuNCs@CNFs had the largest electrochemically active surface.

To investigate the electronic transfer performance of the CuNCs@CNFs, Nyquist plots of the CuNCs@CNFs, CNFs, and bare GCE were measured under the respective open-circuit voltage. Fig. S4 showed that all electrodes possessed well-defined semi-circles that correspond to the charge transfer resistance (R_{ct}). CNFs significantly increase the conductivity of the bare GCE, while the CuNCs decrease the R_{ct} of the CuNCs@CNFs. This is due to the porous CNFs of the CuNCs@CNFs not only providing support and a space-limit environment for CuNCs synthesis but also serving as a conductive media for rapid electron transfer needed for electrochemical sensing.

The electrochemical sensing process of RAC using a CuNCs@CNFs/GCE sensor was explored by measuring the CVs at different scan rates ranging from 10 mV/s to 100 mV/s in the presence of 200 nM RAC (Fig. 2c). It can be seen that the anodic peak current of RAC increases progressively with an increase in scan rate. Whether the electrochemical reaction of RAC is a diffusion or a surface-controlled process can be determined by the following equations:

$$i = av^b \tag{1}$$

$$\log i = b \times \log v + \log a \tag{2}$$

where i and v represent the peak current and scan rate, respectively. In Equation (2), b value is the slope of log i to log v. Generally, when the b value is approximately 0.5, the RAC reaction is a diffusion-controlled process; however, if b is close to 1.0, it represents a surface-controlled process (Zhang et al., 2021). Fig. 2d shows that the b value was 0.846, demonstrating a surface control-dominant process of RAC oxidation on the surface of the CuNCs@CNFs, implying a strong adsorption of CNFs to RAC. To confirm RAC adsorption, CuNCs@CNFs/GCE, CNFs/GCE, and bare GCE were submerged into a 100 nM RAC solution, rinsed, transferred to PBS (0.01 M, pH 7.4) and finally the differential pulse voltammetry (DPV) was recorded. The high peak current signal of the

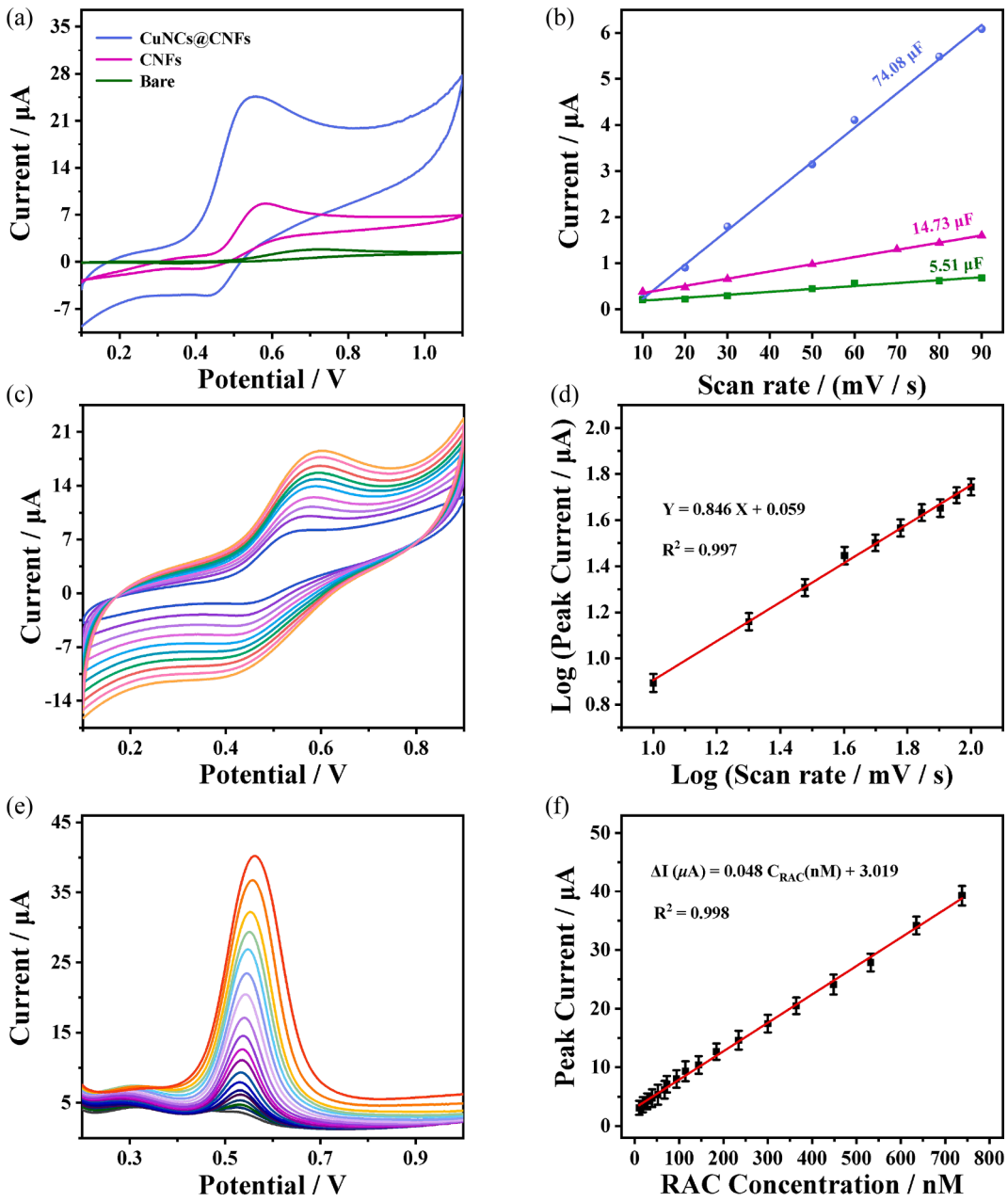

Fig. 2. (a) CV curves towards RAC sensing of different modified electrodes, the electrolyte is 0.01 M PBS (pH 7.4) with 400 nM RAC. (b) Capacitive currents at 0.2 V as a function of scan rates for different electrodes. (c) CV curves of CuNCs@CNFs/GCE at different scan rates with 200 nM RAC in 0.01 M PBS (pH 7.4). (d) Functional relationship of log (peak current) vs log (scan rate). (e) DPV curves of CuNCs@CNFs/GCE at different concentrations RAC in 0.01 M PBS (pH 7.4). (f) Linear calibration curve of the peak currents versus RAC concentrations.

CuNCs@CNFs/GCE and the CNFs/GCE sensors versus that of the bare GCE verified that there is strong adsorption of RAC onto the surface of the CNFs (Fig. S5).

Based on the above results, the enhancement mechanism of CuNCs@CNFs toward RAC sensing was depicted in Scheme 1. RAC with phenolic hydroxyl groups could easily be adsorbed by the CNFs through π-π stacking, resulting in increased concentrations of RAC onto the surface of the electrode, simultaneously shorting the distance between RAC and Cu catalytic active sites on the surface of the CuNCs. Next, the captured RAC was oxidized via the catalytic properties of the CuNCs. The general oxidation process of RAC has been shown in previous reports (Rajkumar et al., 2013; Bai et al., 2014; Baytak et al., 2016). During the sensing process, porous CNFs provided numerous microfluidic channels needed to transport substances like electrolytes and reaction products while promote interfacial charge transfer. Based on the synergistic effects of the CuNCs and the CNFs, the CuNCs@CNFs expressed significantly enhanced RAC sensing performance.

3.3. RAC sensing-performance of the CuNCs@CNFs.

To evaluate the sensor's sensitivity and potential quantitative applications, CuNCs@CNF/GCE was used to detect RAC. DPV responses were recorded in 0.01 M PBS (pH 7.4) containing different RAC concentrations (Fig. 2e). The oxidation peak current increased with increasing RAC concentrations ranging from 0.1 to 800 nM. Using the linear equation: $\Delta I\ (\mu A) = 0.048\ C_{RAC}\ (nM) + 3.019$ ($R^2 = 0.998$) (Fig. 2f) the sensitivity was calculated at 679 μA μM^{-1} cm^{-2}.

The amperometric technique (i-t) is considered a more sensitive detection method than DPV. Therefore, typical i-t curves were obtained by continuously adding specific concentrations of RAC at three different

potentials (Fig. 3a). The i-t curve obtained at 0.55 V showed the highest response, and was selected for the following analysis. Inset of Fig. 3a revealed a rapid electrochemical response time of 1.1 s after RAC injection. As RAC concentration increased, the response current of RAC was proportional to the concentration in the range of 2–850 nM with two linear relationships. The regression equations were: $\Delta I\ (\mu A) = 0.116\ C_{RAC}\ (nM) + 0.011$ ($R^2 = 0.998$) at low RAC concentrations (2–25 nM), and $\Delta I\ (\mu A) = 0.057\ C_{RAC}\ (nM) + 4.307$ ($R^2 = 0.997$) at high RAC concentrations (25–850 nM) (Fig. 3b and c). The calculated sensitivities were 1641 and 806 $\mu A\ \mu M^{-1}\ cm^{-2}$, respectively, with an LOD of 0.05 nM (S/N = 3), which is far below the limited standard (10 $\mu g\ kg^{-1}$) established by the CAC, and further demonstrate this sensor can be used for the detection of RAC in samples. The sensitivity (1641 $\mu A\ \mu M^{-1}\ cm^{-2}$/ 806 $\mu A\ \mu M^{-1}\ cm^{-2}$) can be calculated by the following equation:

$$Sensitivity = S/A$$

Where S and A respectively is the slope of ΔI to C_{RAC} (116 $\mu A\ \mu M^{-1}$/ 57 $\mu A\ \mu M^{-1}$) and the surface area of working electrode (0.07065 cm^{-2}). As a comparison, the sensing ability of the CNFs was shown in Fig. S6, having a much poorer sensitivity of and a lower LOD of 2.28 nM, which further confirmed the high electrocatalytic activity of CuNCs to RAC. As listed in Table 1, the sensitivity of the CuNCs@CNF/GCE sensor in RAC sensing is superior to many other electrochemical methods.

The CuNCs@CNFs/GCE sensors' selectivity was studied using various interference molecules. Considering the normal levels within a biological system, 1.6 mM NaCl, 4 μM Glu and AA, 1 μM UA, DA, Cle, Fen, Sal, and Phe were continuously added to the sensing platform. The addition of 100 nM RAC induced a higher current response than other molecules (Fig. 3d and e), indicating the excellent selectivity of the CuNCs@CNFs/GCE sensor for RAC detection. Except for selectivity, the CuNCs@CNFs/GCE sensor's reproducibility and stability were also examined. To demonstrate the reproducibility of the CuNCs@CNFs/GCE sensor, five parallel electrodes were used to detect 100 nM RAC. The calculated relative standard deviation (RSD) (cumulative variation, which is often used to evaluate the fabrication reproducibility should be smaller than 5 % as an industry standard) was 2.5 % (Fig. 3f), suggesting that the proposed sensor has excellent reproducibility. To investigate the stability of the sensor, 100 nM RAC was detected by the same CuNCs@CNFs modified electrode several times. The RSD of the peak current response values was 2.4 %, revealing good stability of the CuNCs@CNFs/GCE sensor. Furthermore, Fig. S7 shows the response current of the sensor having a decay of 6.02 % than the first test after 25 days, indicating good long-term stability of the sensor.

3.4. Real sample analysis

The practicality of the CuNCs@CNFs/GCE sensor was investigated by detecting RAC in pork, pork liver, chicken, duck, beef and mutton samples. Since RAC was not detectable in these samples (Table 2), different amounts of RAC were added to the sample solutions, and then were detected by both the CuNCs@CNFs/GCE sensor and HPLC to verify the accuracy of this method. The analysis results were summarized in Table 2, the average content of RAC at two spiked concentration levels was close to the content of RAC obtained from HPLC method. Meanwhile, the recoveries of CuNCs@CNFs/GCE sensor at two spiked concentration levels were in the range of 91.39 %-94.58 %, and the recoveries of HPLC ranged from 92.38 % to 95.62 %. Although the recoveries of RAC in meat were different, there were no significant differences among the detection results ($p < 0.05$) (Fig. S8), which revealed that there are no significant differences in the absorption of RAC by different meat, and the results obtained using the CuNCs@CNFs/GCE sensor were consistent with those determined by HPLC, indicating a high potential of this sensor in real sample RAC determination.

4. Conclusions

Herein, we proposed a novel electrochemical sensing platform based on CuNCs@CNFs for the ultrasensitive detection of RAC in food samples. CuNCs@CNFs were synthesized through the in situ carbothermic reduction of Cu^{2+} on porous carbon fibers. The distinct porous structure

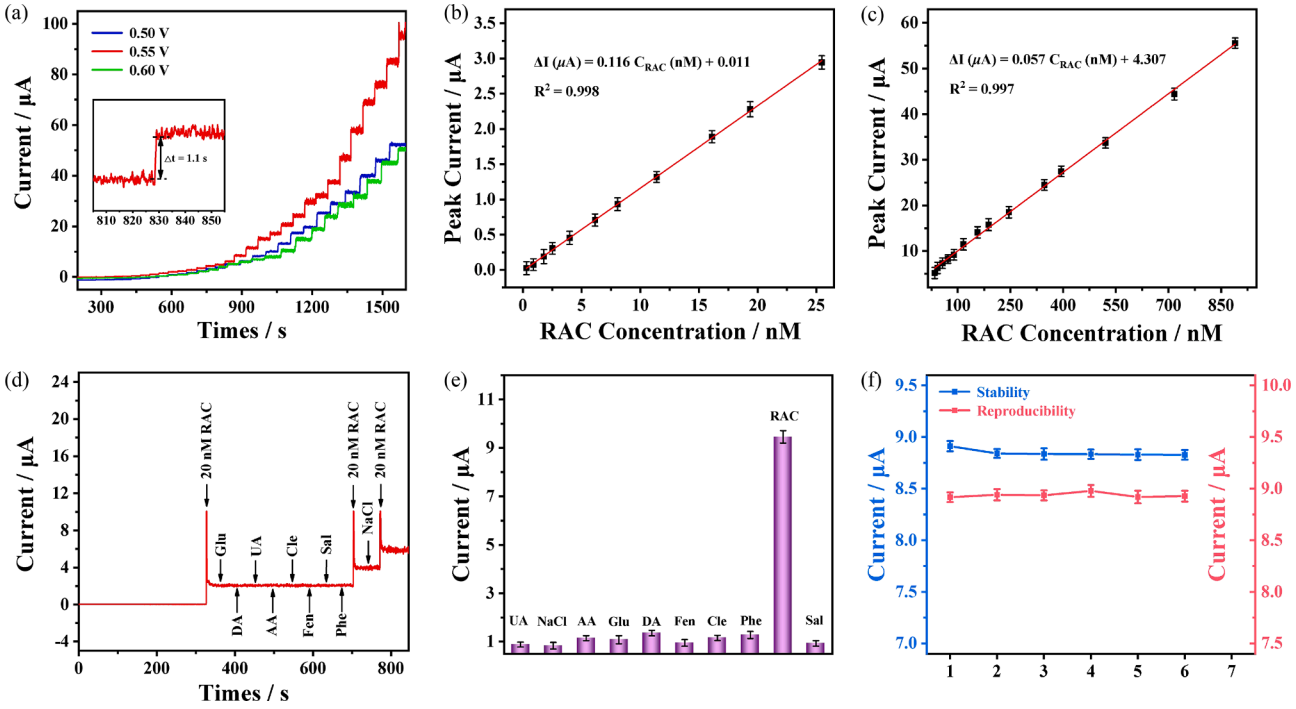

Fig. 3. (a) Amperometric curves of CuNCs@CNFs at different potentials in 0.01 M PBS (pH 7.4) upon continuous injection of RAC with different concentrations, inset is the response time at 0.55 V. (b) Linear calibration curve of the response currents versus the low RAC concentrations corresponding to amperometric curve at 0.55 V. (c) Linear calibration curve of the response currents versus the high RAC concentrations corresponding to amperometric curve at 0.55 V. (d) and (e) Selectivity of CuNCs@CNFs/GCE. (f) Stability (blue) and reproducibility (red) of CuNCs@CNF in presence of 100 nM RAC.

Table 1
Comparison of sensing performance presented in this work and previous works.

Electrode	Detection methods	Linear range (μM)	LOD (nM)	Sensitivity (μA μM^{-1} cm^{-2})	Ref.
G/GNRs[1]/GCE	DPV	0.001–2.7	0.51	84	(Bai et al., 2014)
AB[2]/GCE	DPV	0.00296–5.92	1.6	101.351	(Wang et al., 2015)
ATONPs[3]/CNTs[4]/GCE	DPV	0.01–0.24	3.3	0.558	(Baytak et al., 2016)
$BaTiO_3$@rGOs[5]/SPCE[6]	DPV	0.01–527.19	1.57	–	(Muthumariyappan et al., 2019)
CDs[7]@Au/GCE	DPV	0.029–96.2	3.552	–	(Song et al., 2020)
GO[8]/GCE	DPV	0.074–2.96	56	5.888	(Wu et al., 2012)
OMC[9]/GCE	DPV	0.085–8.0	60	–	(Yang et al., 2014)
NBC[10]-GCE	DPV	0.1–1.75	41	0.416	(Cao et al., 2021)
Poly taurine/ZrO_2/GCE	DPV	1–28	150	3.448	(Rajkumar et al., 2013)
CNTs/GCE	i-t	1–100	340	–	(Bai, 2022)
Au-Nps/AuME[11]	DPV	0.1–380	50	–	(Orooji et al., 2021)
Ti@f-MWCNTs/RDE[12]	i-t	0.01–185	3.8	–	(Keerthi et al., 2022)
CuNCs@CNFs/GCE	i-t	0.002–0.025	0.05	1641	This work
		0.025–0.85		806	

[1] G/GNRs: graphene/gold nanorod; [2]AB: acetylene black; [3]ATONPs: antimony tin oxide nanoparticles; [4]CNTs: carbon nanotubes; [5]rGOs: reduced graphene oxide; [6]SPCE: screen printed carbon electrode; [7]CDs: carbon dots; [8]GO: Graphene oxide; [9]OMC: ordered mesoporus carbon; [10]NBC: Nafion-biochar-supported Cu^{2+}/Cu^{+}; [11]AuME: gold electrode; [12]RDE: rotating disk electrodes.

Table 2
Analysis results of RAC in samples abtained by i-t and HPLC method.

Samples	Added (nM)	i-t (nM) [1]/Recovery	HPLC (nM)[1]/Recovery
Pork	0	not detectable	not detectable
	50	46.10/92.20 %	46.78/93.57 %
	100	92.73/92.73 %	94.12/94.12 %
Pork liver	0	not detectable	not detectable
	50	45.69/91.39 %	46.19/92.38 %
	100	92.32/92.32 %	93.51/93.51 %
Chicken	0	not detectable	not detectable
	50	46.19/92.38 %	47.00/94.00 %
	100	93.12/93.12 %	94.63/94.63 %
Duck	0	not detectable	not detectable
	50	47.29/94.58 %	47.81/95.62 %
	100	94.41/94.41 %	95.13/95.13 %
Beef	0	not detectable	not detectable
	50	46.78/93.57 %	47.09/94.18 %
	100	93.22/93.22 %	93.91/93.91 %
Mutton	0	not detectable	not detectable
	50	46.39/92.79 %	47.50/95.00 %
	100	93.71/93.71 %	94.13/94.13 %

[1] Average value calculated from three determinations.

of the nanocomposite and the synergistic effects between the CuNCs and the CNFs resulted in excellent electrocatalytic activity, and high sensing performance in RAC detection. In addition, the sensor was successfully used to determine RAC in different kinds of meat samples, and obtained satisfactory recoveries. This work provided a reliable and promising platform for the rapid ultrasensitive detection of RAC in foods.

CRediT authorship contribution statement

Yanan Lei: Data curation, Software, Writing – original draft. **Yuhuan Zhang:** Project administration, Formal analysis, Conceptualization, Writing – review & editing. **Li Yuan:** Data curation. **Jianke Li:** Project administration, Conceptualization, Formal analysis.

Declaration of Competing Interest

The authors declare that they have no known competing financial interests or personal relationships that could have appeared to influence the work reported in this paper.

Acknowledgments

The authors gratefully acknowledge the financial supported by the National Key Research and Development Program of China (2019YFD1002400 and 2019YFD1002403), National Natural Science Foundation of China (32102102), China Postdoctoral Science Foundation (2021M692011) and Technological Innovation Guidance Plan of Shaanxi Province (2021QFY07-05).

References

Armstrong, T. A., Ivers, D. J., Wagner, J. R., Anderson, D. B., Weldon, W. C., & Berg, E. P. (2004). The effect of dietary ractopamine concentration and duration of feeding on growth performance, carcass characteristics, and meat quality of finishing pigs. *Journal of Animal Science, 82*, 3245–3253.

Aroeira, C. N., Feddern, V., Gressler, V., Contreras-Castillo, C. J., & Hopkins, D. L. (2021). Growth promoters in cattle and pigs: a review of legislation and implications for human health. *DOI: 10.1080 /87559129.2021.1961268*.

Bai, L. (2022). Electrochemical behavior of salbutamol, clenbuterol, ractopamine and albuterol at CNTs/GCE. *International Journal of Electrochemical Science, 17*(5), Article 220567.

Bai, W., Huang, H., Li, Y., Zhang, H., Liang, B., Guo, R., & Zhang, Z. (2014). Direct preparation of well-dispersed graphene/gold nanorod composites and their application in electrochemical sensors for determination of ractopamine. *Electrochimica Acta, 117*, 322–328.

Bai, Y., Chen, X., & Qi, H. (2022). Characterization and bioactivity of phlorotannin loaded protein-polysaccharide nanocomplexes. *LWT-Food Science and Technology, 117*, 322–328.

Baytak, A. K., Teker, T., Duzmen, S., & Aslanoglu, M. (2016). A novel voltammetric sensor based on carbon nanotubes and nanoparticles of antimony tin oxide for the determination of ractopamine. *Materials Science and Engineering: C, 59*, 368–374.

Cao, L., Ding, Q., Liu, M., Lin, H., & Yang, D. P. (2021). Biochar-supported Cu^{2+}/Cu^{+} composite as an electrochemical ultrasensitive interface for ractopamine detection. *ACS Applied Bio Materials, 4*(2), 1424–1431.

Han, Q., Wang, X., Gao, N., Wang, X., Chen, C., Xu, B., & Ma, F. (2021). Quantitative determination of ractopamine in swine urine using fourier transform infrared (FT-IR) spectroscopy analysis. *Infrared Physics & Technology, 113*, Article 103653.

He, P., Shen, L., Liu, R., Luo, Z., & Li, Z. (2011). Direct detection of beta-agonists by use of gold nanoparticle-based colorimetric assays. *Analytical Chemistry, 83*(18), 6988–6995.

Kang, J. F., Yang, F., Sheng, C., Xu, H., Wang, J. Y., Qing, Y., … Lu, X. H. (2022). CoP nanoparticle confined in P, N Co-doped porous carbon anchored on P-doped carbonized wood fibers with tailored electronic structure for efficient urea electro-oxidation. *Small, 2200950*.

Keerthi, M., Panda, A. K., Wang, Y. H., Liu, X. K., He, J. H., & Chung, R. J. (2022). Titanium nanoparticle anchored functionalized MWCNTs for electrochemical detection of ractopamine in porcine samples with ultrahigh sensitivity. *Food Chemistry, 378*, Article 132083.

Liu, B. L., Cao, Y. L., Zhang, H. Y., Wang, S. Q., Geng, Q., Li, Y. Z., & Dong, F. (2022). Constructing ultrafine Cu nanoparticles encapsulated by N-doped carbon nanosheets with fast kinetics for high-performance lithium/sodium storage. *Chemical Engineering Journal, 446*(1), Article 136918.

Liu, J., He, T., Wang, Q., Zhou, Z., Zhang, Y., Wu, H., & Zhang, Y. (2019). Confining ultrasmall bimetallic alloys in porous N-carbon for use as scalable and sustainable electrocatalysts for rechargeable Zn-air batteries. *Journal of Materials Chemistry A, 7*(20), 12451–12456.

Liu, M. M., Ma, B. A., Wang, Y. P., Chen, E. J., Li, J. L., & Zhang, M. Z. (2022). Research on rapid detection technology for β_2-agonists: Multi-residue fluorescence immunochromatography based on dimeric artificial antigen. *Foods, 11*(6), 863.

Liu, Z., Zhou, Y., Wang, Y., Cheng, Q., & Wu, K. (2012). Enhanced oxidation and detection of toxic ractopamine using carbon nanotube film-modified electrode. *Electrochimica Acta, 74*, 139–144.

Mahmoud, R. S., & Haitham, M. E. (2022). Unraveling novel Cu/Cu_xP@N-doped C composite as effective cocatalyst for photocatalytic hydrogen production under UV and visible irradiation. *Applied Surface Science, 580*, Article 152280.

Muthumariyappan, A., Rajaji, U., Chen, S. M., Baskaran, N., Chen, T. W., & Jothi Ramalingam, R. (2019). Sonochemical synthesis of perovskite-type barium titanate nanoparticles decorated on reduced graphene oxide nanosheets as an effective electrode material for the rapid determination of ractopamine in meat samples. *Ultrasonics Sonochemistry, 56*, 318–326.

Orooji, Y., Asrami, P. N., Beitollahi, H., Tajik, S., Alizadeh, M., Salmanpour, S., … Karimi, F. (2021). An electrochemical strategy for toxic ractopamine sensing in pork samples; twofold amplified nano-based structure analytical tool. *Journal of Food Measurement and Characterization, 15*(20), 4098–4104.

Poo-arporn, Y., Pakapongpan, S., Chanlek, N., & Poo-arporn, R. P. (2019). The development of disposable electrochemical sensor based on Fe_3O_4-doped reduced graphene oxide modified magnetic screen-printed electrode for ractopamine determination in pork sample. *Sensors and Actuators B: Chemical, 284*, 164–171.

Rajkumar, M., Li, Y. S., & Chen, S. M. (2013). Electrochemical detection of toxic ractopamine and salbutamol in pig meat and human urine samples by using poly taurine/zirconia nanoparticles modified electrodes. *Colloids and Surfaces B-biointerfaces, 110*, 242–247.

Shen, Y., Mao, S. D., Chen, F., Zhao, S. C., Su, W. T., Fu, L., … Karimi, F. (2022). Electrochemical detection of Sudan red series azo dyes: Bibliometrics based analysis. *Food and Chemical Toxicology, 163*, Article 112960.

Simon, T., Shellaiah, M., Steffi, P., Sun, K. W., & Ko, F. H. (2018). Development of extremely stable dual functionalized gold nanoparticles for effective colorimetric detection of clenbuterol and ractopamine in human urine samples. *Analytica Chimica Acta, 1023*, 96–104.

Singh, B., Sharma, V., Gaikwad, R. P., Fornasiero, P., Zboril, R., & Gawande, M. B. (2021). Single-atom catalysts: A sustainable pathway for the advanced catalytic applications. *Small, 17*(16), 2006473.

Song, C., Wei, Q. H., Li, H., Gao, H. M., An, J. P., & Qi, B. (2020). Highly sensitive electrochemical sensor based on carbon dots reduced gold nanoparticles for ractopamine detection in pork meat. *International Journal of Electrochemical Science, 15*, 3495–3503.

Sudha, V., Krishnamoorthy, K., Senthil Kumar, S. M., & Thangamuthu, R. (2018). Copper oxide nanosheet modified electrodes for simultaneous determination of environmentally hazardous anions. *Journal of Alloys and Compounds, 764*, 959–968.

Tabuchi, M., Watanabe, K., Morinaga, Y., & Yoshinaga, F. (1998). Acetylation of bacterial cellulose: Preparation of cellulose acetate having a high degree of polymerization. *Bioscience Biotechnology and Biochemistry, 62*(7), 1451–1454.

Vatandost, E., Ghorbani-HasanSaraei, A., Chekin, F., Raeisi, S. N., & Shahidi, S. A. (2020). Green tea extract assisted green synthesis of reduced graphene oxide: Application for highly sensitive electrochemical detection of sunset yellow in food products. *Food Chemistry: X, 6*, Article 100085.

Wang, C. Y., Chen, X., Nakamura, Y., Yu, C. X., & Qi, H. (2020). Fucoxanthin activities motivate its nano/micro-encapsulation for food or nutraceutical application: A review. *Food & Function, 11*(11), 9338–9358.

Wang, R., Wu, K., & Wu, C. (2015). Highly sensitive electrochemical sensor for toxic ractopamine based on the enhancement effect of acetylene black nanoparticles. *Analytical Methods, 7*(19), 8069–8077.

Wang, Y., Wang, M. Q., Lei, L. L., Chen, Z. Y., Liu, Y. S., & Bao, S. J. (2018). $FePO_4$ embedded in nanofibers consisting of amorphous carbon and reduced graphene oxide as an enzyme mimetic for monitoring superoxide anions released by living cells. *Microchimica Acta, 185*(2), 140.

Wang, Y., Zhang, X., Zhao, L., Bao, T., Wen, W., Zhang, X., & Wang, S. (2017). Integrated amplified aptasensor with in-situ precise preparation of copper nanoclusters for ultrasensitive electrochemical detection of microRNA 21. *Biosensors & Bioelectronics, 98*, 386–391.

Wu, C., Sun, D., Li, Q., & Wu, K. (2012). Electrochemical sensor for toxic ractopamine and clenbuterol based on the enhancement effect of graphene oxide. *Sensors and Actuators B: Chemical, 168*, 178–184.

Xia, S., Yu, M., Hu, J., Feng, J., Chen, J., Shi, M., & Weng, X. (2014). A model of interface-related enhancement based on the contrast between Co_3O_4 sphere and cube for electrochemical detection of hydrogen peroxide. *Electrochemistry Communications, 40*, 67–70.

Xiao, Y. X., Ying, J., Chen, J. B., Dong, Y., Yang, X., Tian, G., … Yang, X. Y. (2022). Confined ultrafine Pt in porous carbon fibers and their N-enhancedheavy d-π effect. *Chemistry of Materials, 7*(20), 3705–3714.

Yang, X., Feng, B., Yang, P., Ding, Y., Chen, Y., & Fei, J. (2014). Electrochemical determination of toxic ractopamine at an ordered mesoporous carbon modified electrode. *Food Chemistry, 145*, 619–624.

Yue, X. Y., Zhou, Z. J., Li, M., Jie, M. S., Xu, B. C., & Bai, Y. H. (2022). Inner-filter effect induced fluorescent sensor based on fusiform Al-MOF nanosheets for sensitive and visual detection of nitrofuran in milk. *Food Chemistry, 367*, Article 130763.

Zhang, L., Jia, Q., Liao, G. Q., Qian, Y. Z., & Qiu, J. (2022). A fast method for the simultaneous analysis of 26 beta-agonists in swine muscle with a multi-functional filter by ultra-high performance liquid chromatography-tandem mass spectrometry. *Separations, 9*(5), 121.

Zhang, Y., Guo, C. X., Wu, C., Du, H., Chen, Q., Gao, J. C., & Li, C. M. (2021). Electrochemically tuning $Li_{1+x}FePO_4$ for high oxidation state of rich Li^+ toward highly sensitive detection of nitric oxide. *Electrochimica Acta, 365*, Article 137347.

Zhang, Y., Lu, S. Y., Shi, Z., Zhao, Z. L., Liu, Q., Gao, J. C., & Li, C. M. (2019). A multi-component Cu_2O@$FePO_4$ core-cage structure to jointly promote fast electron transfer toward the highly sensitive in situ detection of nitric oxide. *Nanoscale, 11*(10), 4471–4477.

Zhang, Z., Zhang, Y., Song, R., Wang, M., Yan, F., He, L., & Zhang, H. (2015). Manganese (II) phosphate nanoflowers as electrochemical biosensors for the high-sensitivity detection of ractopamine. *Sensors and Actuators B: Chemical, 211*, 310–317.